JMEPEG (2024) 33:6686–6692
https://doi.org/10.1007/s11665-023-08381-8

1059-9495/$19.00

TECHNICAL ARTICLE

Investigation of Chromium Nitride Precipitation in UNS S39274 Stainless Steel

S.S.M. Tavares, A.R. Pimenta, R.C.P. Loureiro, J. Dille, and L. Malet

Submitted: 8 February 2023 / Revised: 18 May 2023 / Accepted: 22 May 2023 / Published online: 13 June 2023

Chromium nitrides precipitation in a W-alloyed superduplex stainless steel grade UNS S39274 was studied. A microstructure of ferrite, austenite and quenched-in nitrides was produced by solution treatment at 1150 °C followed by water quenching. Although the ferrite to austenite ratio was close to 1:1 after solution treatment, the steel contained a high density of chromium nitrides in the ferrite phase. This intense precipitation could be detected by optical microscopy (LOM), scanning electron microscopy (SEM) and atom force microscopy. Different features were observed comparing specimens electrolytically etched with 40%HNO_3 solution and with 10% oxalic acid solution. The nitrides were also investigated by transmission electron microscopy (TEM), where two types of chromium nitrides were observed: larger CrN/Cr_2N particles and needle-like nanosized CrN particles. The larger nitrides were those observed by SEM and LOM. The nanosized nitrides could only be studied by TEM, where three variants of nanosized precipitates named *V*1, *V*2 and *V*3 were identified. They were found to be coherent with the ferritic matrix and respects the Baker–Nutting orientation relationship with ferrite ($(100)_{CrN}$//$(100)_{\delta-Fe}$; $[110]_{CrN}$//$[001]_{\delta-Fe}$). These fine precipitates provoke pinning of dislocations which is responsible for some hardening of the ferrite phase.

Keywords nitride precipitation, superduplex stainless steel, TEM

1. Introduction

Duplex (DSSs) and superduplex stainless steels (SDSSs) are corrosion resistant alloys selected for uses in harsh conditions (Ref 1, 2). The UNS S39274 grade is a W-alloyed 25%Cr-7%Ni SDSS with pitting resistant equivalent (PREW, (Ref 3)) higher than 40. Cr, Mo, W and N additions provide high resistance to localized corrosion, but the effects of these elements are reduced if they are not completely dissolved in ferritic and austenitic phases.

Nitrogen addition was introduced in austenitic-ferritic steels in the 1970 s, creating the so-called second generation of DSSs (Ref 1). Since that time, the alloys contain nitrogen additions with three main functions: improve the mechanical resistance by solid solution strengthening of austenite; increase the localized corrosion resistance; and act as austenitizing element to obtain a ferrite : austenite proportion close to 1:1 (Ref 4-6).

The chromium nitrides precipitation can occur in modern austenitic-ferritic steels when heated between 700 and 900 °C (Ref 7, 8). In this case, nitrides precipitate with other deleterious phases, such as the intermetallic phases chi (χ) and sigma (σ). Despite the difficulty to separate the effects of the different phases, a study of Sathirachinda et al. (Ref 9) measured the Volta potential of phases precipitated at 800 °C in DSS 2205 and SDSS 2507, and found that Cr_2N is nobler than sigma and austenite phases. However, Cr_2N precipitation creates an adjacent Cr-depleted zone, as determined by computational simulation in the work of Petterson et al. (Ref 10).

Chromium nitrides can also precipitate when the steel is heated to elevated temperatures and rapidly cooled. In this case they are called quenched-in nitrides (Ref 11). Knyazeva and Pohl (Ref 12) claims that the quenched-in nitrides are metastable CrN, and that the precipitation of these particles cannot be suppressed even at cooling rates as high as 2500 °C/s. Also, according to these authors, the Cr_2N precipitates in isothermal annealing in the interval of 550-1000 °C, and has low coherency with the ferrite and austenite phases.

In a recent work of our group (Ref 13), it was found that the increase of solution treatment temperature from 1050 to 1150 °C caused the increase of quenched in nitrides in the ferrite phase of a UNS S39274 steel, with consequences on the corrosion resistance of the alloy. This material is relatively new and much less investigated than the more usual SDSS grades UNS S32750 and S32760. In particular, there is a lack of information about the type, size and morphology of nitrides precipitated in the UNS S39274.

In the present work, chromium nitride precipitation in the same steel solution treated at 1150 °C was investigated by optical microscopy (LOM), scanning electron microscopy (SEM), atomic force microscopy (AFM) and transmission electron microscopy (TEM). The main objective was to characterize the nitrides particles and to show how they are revealed by different etching procedures and techniques.

S.S.M. Tavares, Departamento de Engenharia Mecânica, Universidade Federal Fluminense, Rua Passo da Pátria, 156, Niterói, RJ, Brazil; **A.R. Pimenta**, LISComp, Instituto Federal do Rio de Janeiro, Paracambi, Brazil; **R.C.P. Loureiro**, Departamento de Engenharia Metalúrgica e de Materiais, Laboratório de Caracterização de Materiais, Universidade Federal do Ceará (UFC), Fortaleza, Brazil; and **J. Dille** and **L. Malet**, 4MAT, Materials Engineering, Characterization, Processing and Recycling, Université Libre de Bruxelles, 50 Avenue FD Roosevelt, CP194/03, Brussels, Belgium. Contact e-mail: ssmtavares@id.uff.br.

2. Experimental

The chemical composition of the UNS S39274 SDSS investigated is presented in Table 1.

Specimens of 15 × 15 × 10 mm of the steel were solution treated at 1150 °C for 1 h and water quenched. Specimens for light optical microscopy (LOM), scanning electron microscopy (SEM), and atomic force microscopy (AFM) were prepared by grinding and polishing with diamond pastes (6, 3 and 1 μm) and different electrolytic etchings. The ferrite and austenite were measured by LOM quantitative metallography on specimens etched with Behara's solution (80 ml H_2O, 20 ml HCl, 0.3 g potassium metabisulfite). The austenite/ferrite quantification was performed with Image J software (Ref 14) analyzing 20 image fields. Electrolytic etchings with 10% oxalic acid solution (8 V, 60 s) and with 40%HNO_3 solution (2-3 V, 60 s) were used to prepare specimens for nitrides investigation by LOM, SEM and AFM. The three etchants used are cited in ASTM E-407-15 (Ref 15), but some modifications in solutions compositions, voltage and time of exposition were performed to optimize the results.

The TEM investigations were performed using a Philips CM20 transmission electron microscope operating at 200 kV. The thin foils were prepared by twin-jet electropolishing in a chemical solution of 10% perchloric acid, 20% glycerin and 70% ethanol at 25 V and − 30 °C.

In addition to microstructural analyzes, Vickers microhardness of austenite and ferrite phases were measured with a load of 0.245N (25 gf). Vickers hardness with load 10kgf was also measured.

3. Results and Discussion

Figure 1 shows the LOM image of the specimen solution treated at 1150 °C with ferrite (dark) and austenite (light) elongated in the rolling direction. After the solution treatment, the steel presented a microstructure with (51.3 ± 4.9)% of austenite and (48.7 ± 4.9)% of ferrite, as determined with Image J software.

The Vickers microhardness of ferrite and austenite phases is (273 ± 11) HV0.025 and (246 ± 10) HV0.025, respectively. The Vickers hardness measured with load 10 kgf was (279.4 ± 1.7) HV10, which corresponds to approximately 265 HBN, hence in accordance to the specification ASTM A790-22 for the solution treated UNS S39274 steel (Ref 16).

Figure 2(a-d) shows the microstructure of specimens etched with 40%HNO_3 solution (2-3 V, 60 s) and observed by SEM. Coarse chromium nitride particles were revealed in the ferrite phase, as observed with secondary electrons image (Fig. 2a-c) and backscattered electrons image (Fig. 2d). In Fig. 2(c) and (d) the particles appear like randomly oriented lamellae. It is worth noting that, even having an austenite content close to 50%, which is considered the optimum balance, the UNS S39274 steel studied has a high density of nitrides as result to the solution treatment at 1150 °C.

The etching with 10% oxalic acid solution (8 V, 60 s) provoked intense attack of the ferrite phase where the nitrides precipitated, creating numerous holes or dimples, as it can be observed on SEM images from Fig. 3(a-d). Ferrite grain and sub-grain boundaries were also attacked.

Fig. 4(a-b) shows comparatively how the microstructures revealed by etching with 40%HNO_3 (3 V, 30 s) and with 10% oxalic acid solutions (8 V, 60 s) are observed by LOM. The intensity of the attack depends on the parameters of electrolytic etching, such as voltage and etching time. The increase of these two parameters intensifies the attack around nitrides and carbides (Ref 13).

When the microstructures are observed by Atomic Force Microscopy (AFM), it is possible to see that the etching with 40% HNO_3 corrodes more the ferrite phase than the austenite (Fig. 5a-b). Also, the 3-D images show the lamellae of chromium nitrides inside the ferrite, and the topography suggests that they were much less corroded by the etching than ferrite. On the other hand, the AFM analysis of the specimen etched with 10% acid oxalic solution (Fig. 5c-d) shows that austenite is preferentially corroded, and that several pits are present in ferrite due to the chromium nitrides.

The bright-field TEM images of Figure 6(a-d) show that within the ferrite grains, precipitates of 2 different sizes are observed: nanosized precipitates as well as coarser precipitates. The coexistence of 2 kind of precipitates was already reported by Pettersson et al. (Ref 17) in a SDSS UNS S32750. The coarser precipitates are shown in detail on Fig. 6(c-d). The morphology and size are compatible with the lamellae precipitates observed by SEM and AFM in specimens etched with 40%HNO_3. Pettersson et al. (Ref 17) identified the coarser precipitates as a mixture of Cr_2N and CrN.

The nanosized particles were investigated in more detail. TEM bright-field image (Fig. 7a) reveals three variants of nanosized precipitates named *V*1, *V*2 and *V*3. To our knowledge, this observation has never been mentioned in the literature for superduplex stainless steels but is well docu-

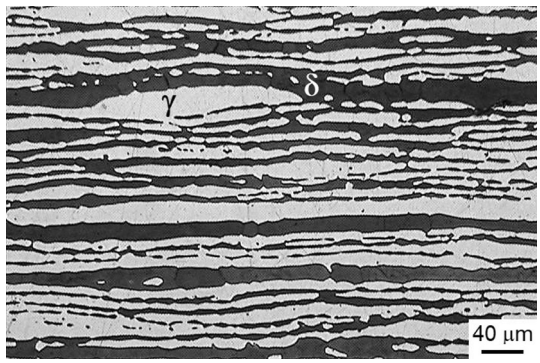

Fig. 1 LOM image of specimen solution treated at 1150 °C (Behara's etching)

Table 1 Chemical composition (wt.%) of UNS S39274 studied

C	Cr	Ni	Mo	W	S	P	N	Fe
0.028	24.79	6.600	3.220	1.750	0.002	0.017	0.255	Bal.

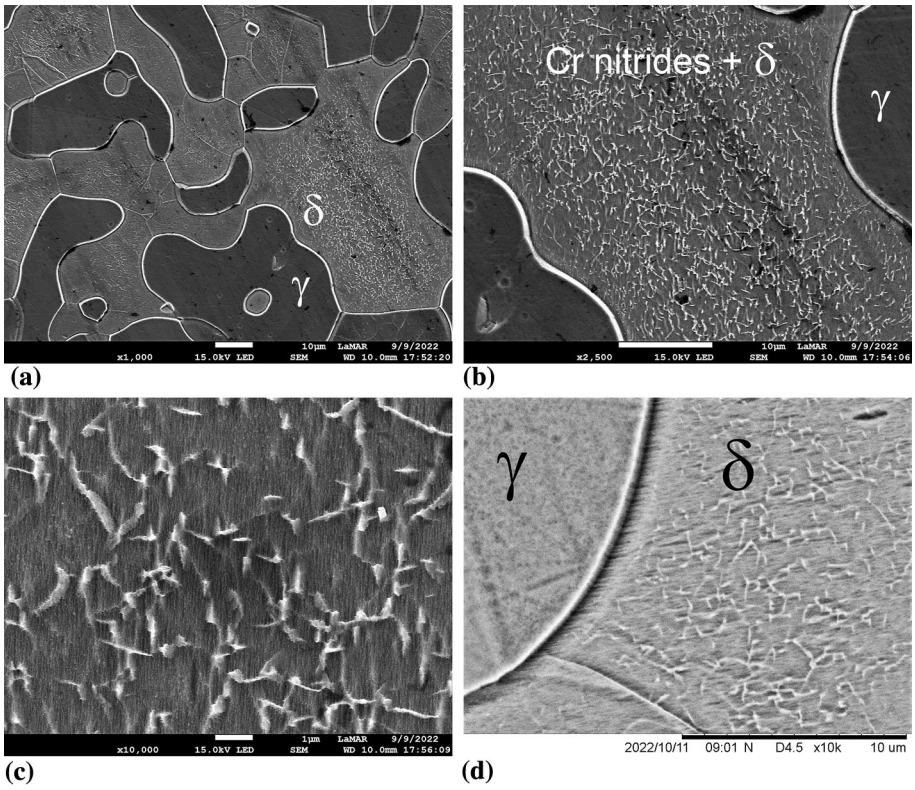

Fig. 2 SEM images of the specimen etched with 40% HNO_3 solution (electrolytic, 3 V, 30 s): (a-c) secondary electrons image (d) backscattered electrons image

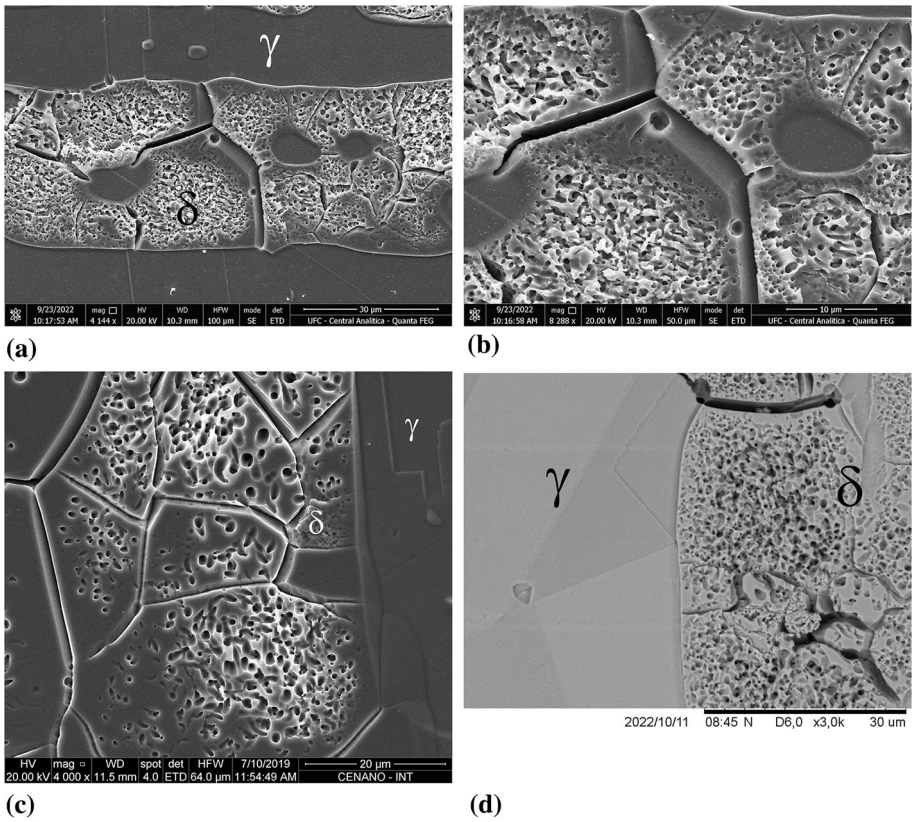

Fig. 3 SEM images of the specimen etched with 10% oxalic acid solution (electrolytic, 8 V, 60 s): (a-c) secondary electrons image (d) backscattered electrons image

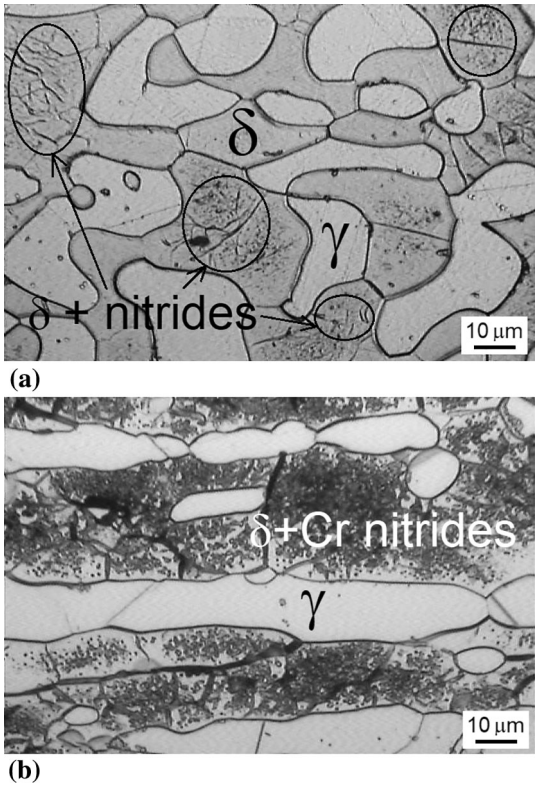

Fig. 4 LOM images of specimens etched with electrolytic etching with: (a) 40%HNO3 solution and (b) 10% oxalic acid solution

mented for nitrided ferritic steels (Ref 18-20). In a nitrided layer, three CrN variants, orthogonal to each other, coexist and respect the Baker–Nutting orientation relationship (OR) with ferrite:

$$(100)_{\mathrm{CrN}}//(100)_{d-\mathrm{Fe}}; [110]_{\mathrm{CrN}}//[001]_{d-\mathrm{Fe}}$$

The Baker–Nutting (B–N) relation has been previously observed in the plasma-nitrided layer of a ferritic Fe-18%Cr steel, among with other ORs, such as Kurdjumov–Sachs (K–S) and Nishyiama–Wassermann (N–W) (Ref 20). The ORs between CrN and α-bcc phase were also investigated by TEM in austenitic stainless steels submitted to nitriding, but only K–S and N–W ORs were reported (Ref 21, 22).

The B-N orientation relationship matches rather closely the atomic positions within the habit plane, but induces a strong misfit in the perpendicular direction, leading to needle-like or disc-like morphologies for the precipitates (Ref 23).

On Fig. 7(a), variants 1 and 2 appear as rods, whereas variant 3 appears as points. This indicates that the CrN precipitates have a needle-like morphology. Moreover, the comparison of the bright-field image with the electron diffraction pattern (Fig. 7b) of the same region reveals that the CrN needles are orthogonal to each other and parallel to ferrite 100 direction. Variant 1 is parallel to the ferrite [100] direction, whereas variant 2 is parallel to the ferrite [010] direction. Variant 3 appears as a point on the TEM bright-field image and, thus, is perpendicular to the thin foil and parallel to the [001] ferrite zone axis.

Figure 8 shows some dislocations pinned by fine CrN precipitates. The lengths of the needles are smaller than 100 nm. The « coffee-bean contrast » observed in ferrite

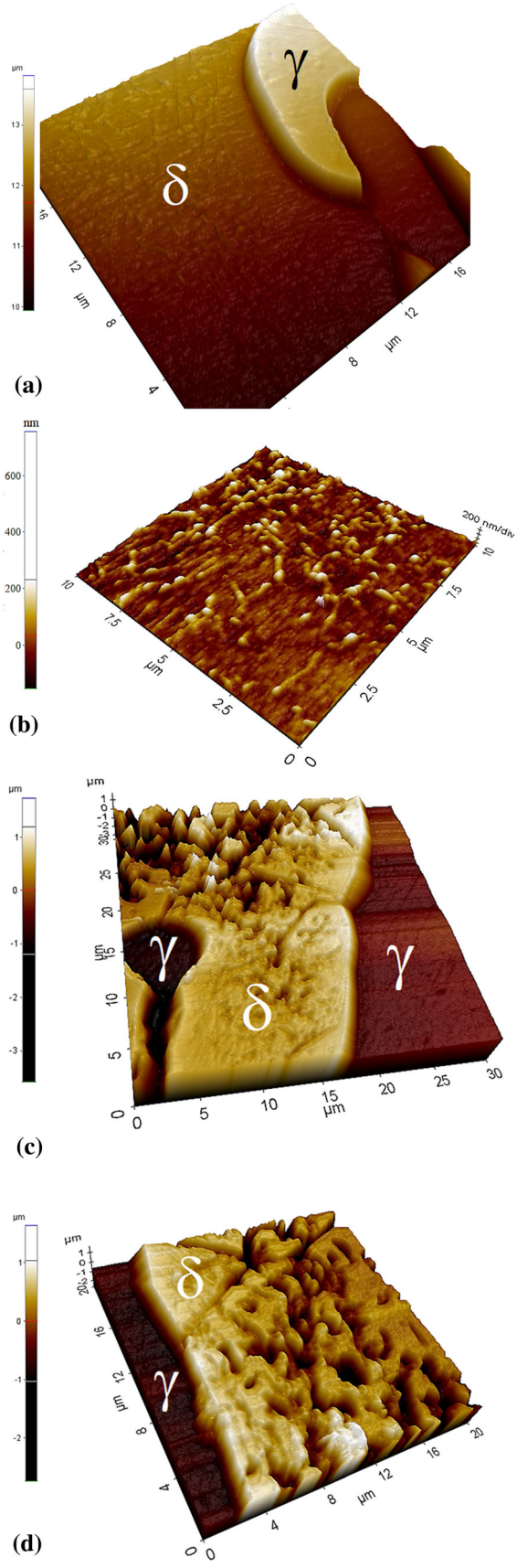

Fig. 5 3D AFM images: (a) General view and (b) Ferrite phase and nitrides in specimen etched with 10%HNO_3 solution (3 V, 30 s); (c-d) Specimen etched with 10% oxalic acid solution (9 V, 60 s)

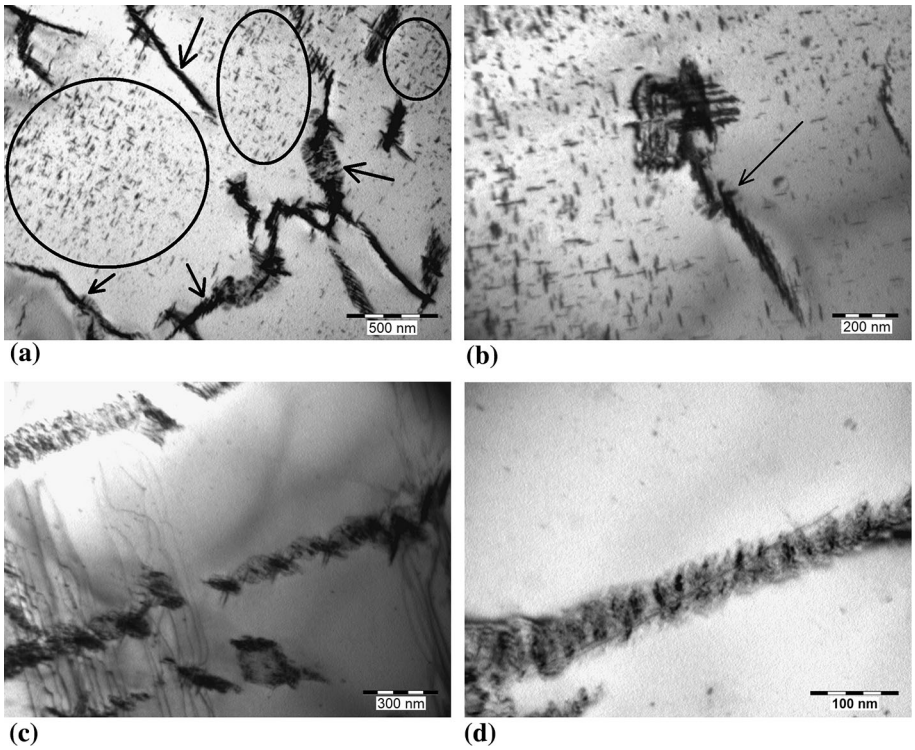

Fig. 6 Bright-field TEM images: (a-b) coarse and fine nitride particles, identified by arrows and circles, respectively; (c-d) coarse Cr_2N/CrN particles in detail

regions adjacent to CrN precipitates is due to the strain field induced by the coherency of the interface between ferrite and CrN precipitate.

The fact of ferrite is harder than austenite in the steel studied is curious because it was not observed in other steels. In duplex UNS S32205 and superduplex UNS S32750 steels, the austenite was harder than ferrite, and this was attributed to the effect of solid solution hardening by nitrogen in the austenite (Ref. 8). However, in the UNS S39274 the high density of nitrides found in the ferrite makes believe that there is less nitrogen in austenite and its effect of hardening this phase by solid solution is somewhat decreased, when compared to the other steels. On the other hand, coherent precipitation of nanosized precipitates with respect to the ferritic matrix can also contribute to explain the higher microhardness of ferrite compared to austenite in the material solution treated at 1150 °C.

The ferrite phase was also harder than the austenite phase in samples solution treated at 1100 and 1050 °C (Ref 13). However, the increase of the solution treatment temperature caused a decrease of microhardness of ferrite, which is an unexpected result, since the Cr nitrides density was raised (Ref 13). Further investigation with specimens treated at 1050 and 1100 °C is necessary to understand this behavior.

4. Conclusion

Specimens of UNS S39274 superduplex stainless steel were solution treated at 1150 °C followed by water cooling, and presented a microstructure of 51.3% of austenite, 48.7% of ferrite, and chromium nitrides precipitated in the ferrite phase. Two sizes and morphologies of chromium nitrides were observed by TEM: nanosized precipitates and coarser lamellar precipitates. These last ones were also observed by SEM in specimens electrolytically etched with 40%HNO_3 solution (3 V, 30 s). The AFM analysis revealed that this etching caused a corrosion of ferrite and preserved austenite, while the lamellar nitrides inside the ferrite were highlighted. Etching with 10% acid oxalic solution indirectly revealed the presence of nitrides causing micro-pitting and intergranular attack of the ferrite phase, as observed by SEM and AFM. Nanosized CrN precipitates were only observed by TEM. These are needle-like particles, with less than 100 nm of length. They were found to be coherent with the ferritic matrix and respect the Baker–Nutting orientation relationship with ferrite: $((100)_{CrN}//(100)_{\delta-Fe}; [110]_{CrN}//[001]_{\delta-Fe})$.

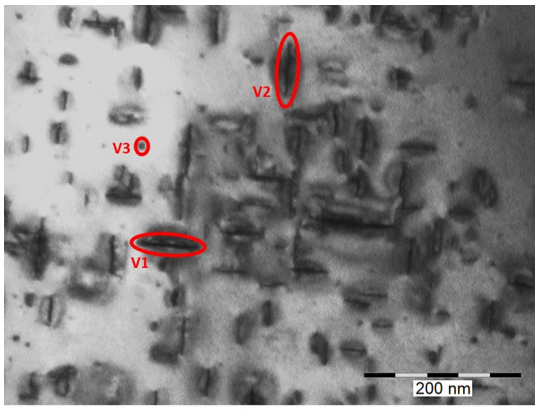

(a)

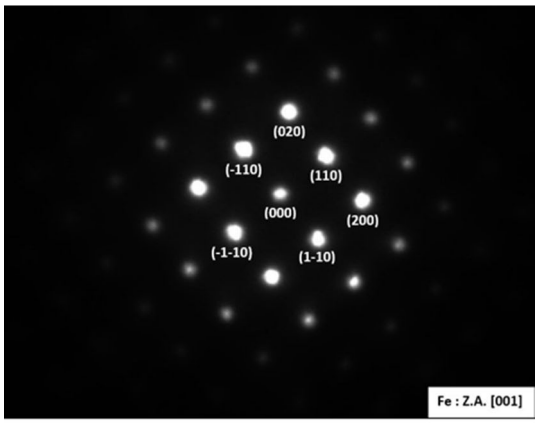

(b)

Fig. 7 (a) Bright-field TEM image of nanosized CrN precipitates (b) Electron diffraction pattern of the same region (zone axis: [001] ferrite)

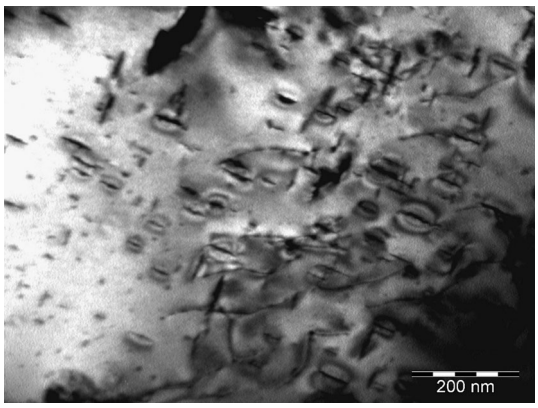

Fig. 8 Bright-field TEM image of CrN nanosized precipitates with "coffee-bean" contrast

Acknowledgments

Authors acknowledge Brazilian research agencies CNPq (308244/2022-2) and FAPERJ (E-26/211.412/2021; E-26/200.122/2023; E-26/200.423/2023) for financial support, and CENANO/INT for electron microscopy facilities.

Data Availability

The raw/processed data required to reproduce these findings can be shared under demand.

References

1. R.N. Gunn, *Duplex Stainless Steels: Microstructure, Properties and Applications*, 1st ed. Woodhead Publishing, 1997
2. J.-O. Nilsson, Super Duplex Stainless Steels, *Mater. Sci. Technol.*, 1992, **8**(8), p 685–700.
3. NACE, *NACE ISO 15156-3 Petroleum and Natural Gas Industries - Materials for Use in H2S-Containing Environments in Oil and Gas Production: Part 3: Cracking-Resistant CRAs (Corrosion- Resistant Alloys) and Other Alloys*, NACE International, 2015
4. W. Horvath, B. Tabernig, E. Werner, and P. Uggowitzer, Microstructures and Yield Strength of Nitrogen Alloyed Super Duplex Steels, *Acta Mater.*, 1997, **45**(4), p 1645–1654.
5. R.B. Bhatt, H.S. Kamat, S.K. Ghosal, and P.K. De, Influence of Nitrogen in the Shielding Gas on Corrosion Resistance of Duplex Stainless Steel Welds, *J. Mater. Eng. Perform.*, 1999, **8**(5), p 591–597.
6. A.R. Pimenta, M.G. Diniz, G. Perez, and I.G. Solórzano-Naranjo, Nitrogen Addition to the Shielding Gas for Welding Hyper-Duplex Stainless Steel, *Soldag. Insp.*, 2020, **25**, p e2512.
7. L. Pezzato, M. Lago, K. Brunelli, M. Breda, and I. Calliari, Effect of the Heat Treatment on the Corrosion Resistance of Duplex Stainless Steels, *J. of Materi Eng and Perform*, 2018, **27**(8), p 3859–3868.
8. P.H.R. Pecly, B.B. Almeida, G. Perez, A.R. Pimenta, and S.S.M. Tavares, Microstructure, Corrosion Resistance, and Hardness of Simulated Heat-Affected Zone of Duplex UNS S32205 and Superduplex UNS S32750 Stainless Steels, *J. of Materi Eng and Perform*, 2023 https://doi.org/10.1007/s11665-022-07784-3
9. N. Sathirachinda, R. Pettersson, S. Wessman, and J. Pan, Study of Nobility of Chromium Nitrides in Isothermally Aged Duplex Stainless Steels by Using SKPFM and SEM/EDS, *Corros. Sci.*, 2010, **52**(1), p 179–186.
10. N. Pettersson, R.F.A. Pettersson, and S. Wessman, Precipitation of Chromium Nitrides in the Super Duplex Stainless Steel 2507, *Metall and Mat Trans A*, 2015, **46**(3), p 1062–1072.
11. E. Bettini, U. Kivisäkk, C. Leygraf, and J. Pan, Study of Corrosion Behavior of a 2507 Super Duplex Stainless Steel: Influence of Quenched-in and Isothermal Nitrides, *Int. J. Electrochem. Sci.*, 2014, **9**, p 61–80.
12. M. Knyazeva and M. Pohl, Duplex Steels: Part II: Carbides and Nitrides, *Metallogr. Microstruct. Anal.*, 2013, **2**(5), p 343–351.
13. S.S.M. Tavares, A.C. Gonzaga, J.M. Pardal, J.N. Conceição, and E.O. Correa, Nitrides Precipitation and Preferential Pitting Corrosion of Ferrite Phase in UNS S39274 Superduplex Stainless Steel, *Metallogr. Microstruct. Anal.*, 2020, **9**(5), p 685–694.
14. C.A. Schneider, W.S. Rasband, and K.W. Eliceiri, NIH Image to ImageJ: 25 Years of Image Analysis, *Nat. Methods*, 2012, **9**(7), p 671–675.
15. ASTM, *E407: Standard Practice for Microetching Metals and Alloys*, ASTM International, 2015
16. ASTM, *"A790/A790M Standard Specification for Seamless and Welded Ferritic/Austenitic Stainless Steel Pipe*, ASTM International, USA, 2022
17. N. Holländer Pettersson, D. Lindell, F. Lindberg, and A. Borgenstam, Formation of Chromium Nitride and Intragranular Austenite in a Super Duplex Stainless Steel, *Metall. Mater. Trans. A.*, 2019, **50**(12), p 5594–5601.
18. M. Sennour, C. Jacq, and C. Esnouf, Mechanical and Microstructural Investigations of Nitrided Fe-Cr Layers, *J. Mater. Sci.*, 2004, **39**(14), p 4533–4541.
19. J.-N. Locquet, R. Soto, L. Barrallier, and A. Charaï, Complete TEM Investigation of a Nitrided Layer for a Cr Alloy Steel, *Microsc. Microanal. Microstruct.*, 1997, **8**(4-5), p 335–352.
20. G. Miyamoto, A. Yonemoto, Y. Tanaka, T. Furuhara, and T. Maki, Microstructure in a Plasma-Nitrided Fe-18 Mass% Cr Alloy, *Acta Mater.*, 2006, **54**(18), p 4771–4779.

21. X.L. Xu, L. Wang, Z.W. Yu, and Z.K. Hei, Microstructural Characterization of Plasma Nitrided Austenitic Stainless Steel, *Surf. Coat. Technol.*, 2000, **132**(2-3), p 270–274.
22. Q.W. Ye, Y. Li, M.Y. Zhang, S.Z. Zhang, Y.J. Bi, X.P. Gao, and Y.Y. He, Electrochemical Behavior of (Cr, W, Al, Ti, Si)N Multilayer Coating on Nitrided AISI 316L Steel in Natural Seawater, *Ceram. Int.*, 2020, **46**(14), p 22404–22418.
23. O. Skiba, A. Redjaïmia, J. Dulcy, J. Ghanbaja, G. Marcos, N. Caldeira-Meulnotte, and T. Czerwiec, A Proper Assessment of TEM Diffraction Patterns Originating from CrN Nitrides in a Ferritic Matrix, *Mater. Charact.*, 2018, **144**, p 671–677.